

# Handover Management in UAV Networks with Blockages

Neetu R.R., Gourab Ghatak and Vivek Ashok Bohara

**Abstract**—We investigate the performance of unmanned aerial vehicle (UAV)-based networks in urban environments characterized by blockages, focusing on their capability to support the service demands of mobile users. The UAV-base stations (UAV-BSs) are modeled using a two-dimensional (2-D) marked-Poisson point process (MPPP), where the marks represent the altitude of each UAV-BS. Leveraging stochastic geometry, we analyze the impact of blockages on network reliability by studying the meta distribution (MD) of the signal-to-interference noise ratio (SINR) for a specific reliability threshold and the association probabilities for both line-of-sight (LoS) and non-line-of-sight (NLoS) UAV-BSs. Furthermore, to enhance the performance of mobile users, we propose a novel cache-based handover management strategy that dynamically selects the cell search time and delays the received signal strength (RSS)-based base station (BS) associations. This strategy aims to minimize unnecessary handovers (HOs) experienced by users by leveraging caching capabilities at user equipment (UE), thus reducing latency, ensuring seamless connectivity, and maintaining the quality of service (QoS). This study provides valuable insights into optimizing UAV network deployments to support the stringent requirements in the network, ensuring reliable, low-latency, and high-throughput communication for next-generation smart cities.

**Index Terms**—UAV, Blockages, SINR Meta distribution, Handover management, Caching, Urban cities

## I. INTRODUCTION

UNMANNED aerial vehicles equipped with remote radio heads (RRHs) function as relays and aerial base stations [1]. With continuous advancements in drone technology, employing UAVs as airborne BSs offers a cost-effective and scalable solution to enhance coverage and improve QoS for end-users [2] - [4]. They can provide on-demand connectivity and extend network coverage to underserved or temporarily congested urban areas. Urban environments, however, present unique challenges for UAV networks, such as blockages, user mobility, and the increasing demand for reliable, low-latency communications [5]. With the rapid growth of smart cities and applications requiring real-time data processing, such as autonomous driving and mobile gaming, ensuring uninterrupted service is critical [6]. Addressing these challenges is vital, as they significantly impact the development and effectiveness of next-generation wireless networks. This research focuses on enhancing UAV network reliability and performance in urban settings by improving connectivity in poorly covered areas, meeting growing mobile data demands, and utilizing

device caching for better service continuity and efficiency [7]. These efforts lay the foundation for scalable and adaptive UAV deployments in smart cities. Additionally, performing a thorough blockage analysis during the deployment planning of UAV-BSs is essential to maintain stable and reliable communication links with ground users. The impact of blockages must also be a primary consideration when developing association strategies in heterogeneous networks [8]. Despite their potential, studying UAV networks in urban environments is inherently complex due to the stochastic nature of blockages, the dynamics of user mobility, and the need to maintain consistent QoS [9]. Integrating device caching capabilities and optimizing UAV placement and handover strategies further adds to this complexity.

Consequently, in the proposed work, we address the challenges posed by urban blockages in UAV-based cellular networks, which severely impact LoS connections essential for smart city applications. By leveraging stochastic geometry, we model these blockages and analyze network reliability through the MD of SINR, offering a comprehensive evaluation of QoS. To address frequent handovers caused by user mobility, we propose a cache-enabled HO management scheme that utilizes caching at the UE to reduce unnecessary handovers, lower latency, and enhance throughput. The proposed cache-enabled handover management strategy provides a practical approach to ensuring seamless connectivity, meeting stringent QoS requirements, and dynamically adapting to user mobility and blockage scenarios.

### A. Related Works

Drones as relays and aerial BSs gain interest due to their flexibility in deployment and flying capabilities [10]. Deploying UAVs in regions lacking terrestrial base stations (TBSs) to enhance capacity and coverage has been broadly investigated in the literature e.g., [11] - [13]. A number of studies have so far investigated incorporating UAVs into the network, and many of them have adopted stochastic geometry tools to analyze the network performance [14], [15]. The authors in [16] investigated the feasibility of integrating two applications of UAVs, such as aerial BSs and data delivery, serving multiple IoT clusters on the ground. They proposed a performance metric, data delivery efficiency, to deliver the data to the clusters in less time. They proposed an algorithm to jointly optimize the minimum round trip time to serve the clusters and maximize the delivered data to the clusters.

1) *Blockage Analysis*: The authors in [17] used the concepts of random shape theory to model the blockages with random sizes, shapes, and orientations. The blockages are

Neetu R.R. and Vivek Ashok Bohara are affiliated with the Department of Electronics and Communication Engineering, IIT-Delhi, India. (Email: neetur, vivek.b@iitd.ac.in). Gourab Ghatak is with the Department of Electrical Engineering, IIT Delhi, India. (Email: ggghatak@ee.iitd.ac.in). This research is funded by the IIT Palakkad Technology IHub Foundation Doctoral Fellowship IPTIF/HRD/DF/026.

considered as Poisson point process (PPP), and they incorporated the heights of the blockages for the network analysis. They study the behavior of the probability of the LoS links and its dependency on the length of the link. They analyzed the coverage probability and achievable rate at the user in the presence of blockages. In [18], the authors proposed a power control strategy for urban UAV networks that mitigates interference by muting the transmissions of interfering UAVs. The proposed strategy includes a power control coefficient that is dependent on environmental blockage parameters and uses stochastic geometry to derive coverage probability and network connectivity. The authors in [19] study multiple types of blockages in the network, which affect the coverage performance of single-swarm mmWave UAV networks. The effect of blockages, such as static, dynamic, and self-blockages, on the system performance are jointly considered. They analyzed the effect of all these blockages on the coverage probability, average LoS probability, and average path loss for UAVs by varying the number of UAVs and heights of the UAVs. They observed that static blockage and self-blockage exert a predominant influence on these metrics, and the effect of self-blockage can be mitigated by flying the UAVs at a sufficiently high altitude.

2) *Fine-Grained Analysis of UAV Networks*: Meta distribution and reliability analysis in traditional cellular networks is studied in various literature [20]- [22]. The fine-grained analysis in UAV-enabled networks is performed in [23], which investigates the SINR MD performance of UAVs equipped with either steerable or fixed directional antennas using stochastic geometry. They derived the distribution of the off-boresight angle (OBA) and calculated the moments of the conditional success probability (CSP). Additionally, they obtained the mean local delay and SINR MD for various environmental scenarios. The study also explored the asymptotic behavior of the association probability and the moments of the CSP. Moreover, the authors in [24] analyzed the downlink performance of the UAV network from the perspective of each link other than spatial averaging. The authors consider two types of user distributions, PPP and Matérn cluster process (MCP), and observed the MD for UAV-enabled HetNet and TBS only network. The authors the advantages and disadvantages of deploying UAVs and the height and density at which the UAVs should be deployed in the network depending on different environmental scenarios. The authors in [25] study the downlink rate meta-distribution in a typical UAV in a cellular-connected UAV network. Considering the Nakagami-m fading for the LoS transmissions, the authors derive LoS probability and observe the impact of rate threshold and link reliability threshold on rate MD.

3) *Handover Analysis*: HO management using different schemes, e.g., velocity-aware HO management [26], route-aware HO management [27] and skipping alternatively [22] and other schemes have been discussed in the literature [6] - [29]. Different from the above literature, the authors in [30] proposed a periodic handover skipping strategy that introduces a defined skipping period after each handover. They used stochastic geometry to analyze the handover rate and the expected download rate at the user end. In addition, [30]

also defined a utility metric, which is a function of the HO rate and achievable download rate, and compared the utility function for different distributions of user velocity. It is observed that when the user's velocity is very high, the proposed strategy outperforms conventional methods. In [31], the authors investigated a three-dimensional (3-D) mobile UAV network and analyzed the handover and coverage probability using stochastic geometry tools. They discussed two types of association strategies of the typical user in the origin, such as strongest average RSS association and nearest distance association. The authors analyzed the handover probability and coverage probability of these two association strategies. They observed that the RSS based strategy performs better than the distance-based associations, and there exists an optimal UAV density and altitude to maximize the coverage probability. In our work in [32], we study a handover management scheme by leveraging device caching in vehicles where the locations of small base stations (SBSs) are distributed according to a one-dimensional (1-D) homogeneous Poisson point process (HPPP). We analyze a handover-skipping strategy by storing the necessary data at the vehicle terminal to reduce unnecessary handovers while maintaining the quality of experience (QoE) at the user end. We derive the analytical expressions for caching distance, HO rate, and the average throughput experienced by the vehicle terminal. We perform a spatiotemporal expectation to derive the effective average rate experienced by the vehicle terminal.

## B. Motivation and Contribution

The deployment of UAV-BSs has emerged as a promising solution for enhancing network performance in dynamic, blockage-prone urban environments. However, most prior studies assume UAVs are deployed at fixed altitudes, limiting their mobility to a single axis. In this paper, we overcome this limitation by modeling UAV-BSs as a 2-D MPPP, representing their locations in 3-D space with random distributions over  $\mathbb{R}^2$  in the horizontal plane and along the vertical axis. Different from our conference version in [33], this study extends the analysis to urban scenarios characterized by blockages and mobile users. Notably, this study explores the MD of SINR for a specified reliability threshold in networks where UAVs are distributed as a 2-D MPPP, considering the impact of blockages, is an aspect which is not previously addressed in the literature. Moreover, none of the literature has proposed a novel HO management scheme that leverages the caching capabilities of UEs. This approach aims to mitigate handover delays and enhance QoS in a 2-D MPPP UAV network under blockage conditions.

Motivated by this, we investigate a 2-D MPPP in which the altitudes of the UAV-BSs are represented as marks. By leveraging stochastic geometry, this work analyzes SINR MD for a specific reliability threshold in the presence of blockages. This work proposes a novel cache-enabled HO management scheme, leveraging caching at UE to minimize unnecessary HOs, reduce delays, and ensure seamless service continuity.

The significant contributions are outlined as follows:

- 1) We develop a novel framework to represent UAV-BS locations in 3-D space, where the 2-D positions follow

a MPPP and altitudes are modeled as random marks in an urban network with blockages. We derive analytical expressions for the distance distributions to the nearest LoS and NLoS UAV-BSs from the typical user, as well as for the probabilities of user association.

- 2) Given the proposed network topology, we analyze the MD of SINR for a specified reliability threshold in UAV-based urban networks. Our study investigates the impact of varying blockage densities and UAV deployment densities, determining the optimal deployment density that enhances overall network reliability while minimizing the mean local delay.
- 3) Additionally, we propose a cache-enabled HO management algorithm that leverages caching capabilities at UE to minimize unnecessary HOs, reduce HO delays, improves QoS and energy efficiency. This strategy dynamically adjusts cell search intervals and employs an HO skipping mechanism to enhance the user experience in dense UAV urban networks with blockages.
- 4) *Insights:*

- We observe that increasing network density does not consistently enhance LoS associations. On the contrary, higher densities expand the NLoS regions relative to LoS regions, thereby reducing the number of LoS connections from the typical user.
- Contrary to traditional assumptions, for higher deployment density of UAV-BSs, blockages can enhance the network performance by blocking the interference in the network. In regions with lower blockage levels, fewer UAVs are demanded, while regions with higher blockage levels demand a larger number of UAVs to achieve improved network performance.
- The intensity and distribution of blockages play a crucial role in determining the optimal deployment altitude for UAV-BSs. In regions with sparse blockages, lower altitudes improve performance by maximizing LoS connections, whereas in densely blocked areas, higher altitudes are preferable to mitigate obstructions and enhance connectivity.

The rest of the paper is organized as follows. In Section II, we discuss the system model and summarize the objectives. In Section III, we discuss the appropriate distance distributions to the nearest UAV-BSs and association probabilities. In Section IV, MD-based analytical framework and CSP analysis is performed. In Section V, a cache-based handover skipping algorithm is proposed and derived HO rate and average throughput. Section VI validates the analytical framework and presents numerical results that highlight key aspects of the network. Finally, the conclusions are discussed in Section VII.

## II. SYSTEM MODEL

### A. Network Model

We consider a downlink UAV-based network in urban environments characterized by blockages, designed to support the connectivity demands of smart device users. The network consists of UAV-BSs modeled as a 2-D homogeneous PPP,  $\Phi_U$  on  $\mathbb{R}^2$ , with intensity  $\lambda_u$ . Each point of  $\Phi_U$  has an

associated mark representing the altitude of the UAV-BSs. We assume the marks are uniformly distributed between  $h_{min}$  and  $h_{max}$ . This configuration forms a 2-D MPPP. We assume that the UAV-BSs are equipped with down-tilted omnidirectional antennas serving single-antenna users. Without loss of generality, utilizing the stationarity and isotropy properties of the PPP [34], we consider a user moving in a straight line within a 2-D plane that passes through the origin at a velocity  $v$ . Let  $\mathbf{X}_0 \in \Phi_U$  represent the 2-D location of the UAV-BS at an altitude  $h_0$  to which the user is connected at a specific time. Without loss of generality, leveraging the ergodicity property of the PPP [34], we assume the user to be located at the origin at that time. By averaging over various realizations, this user is treated as the typical user. Using the Uu interface [35], the typical user associates with the UAV-BS providing the maximum received power, assessed through the estimated received signal strength indicator (RSSI) measurements in the downlink. Each UAV-BS has a dedicated backhaul link to the centralized network. Additionally, we consider that orthogonal frequency allocation is employed to aggregate users [36]. Since the altitudes of UAV-BSs are uniformly distributed between  $h_{min}$  to  $h_{max}$ , the cell boundaries are formed by weighted Poisson Voronoi tessellation in the 2-D plane. Another tier of TBSs can easily be incorporated into the network without any change in the mathematical analysis.

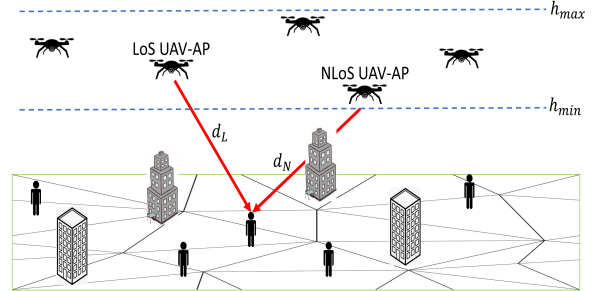


Fig. 1. An illustration of the system model in which the user is served by either LoS or NLoS UAV-BS.

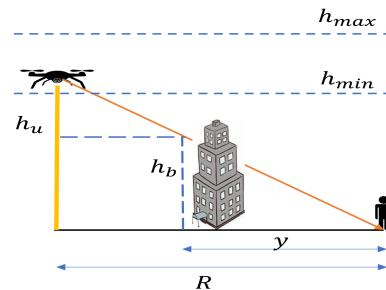


Fig. 2. A building intersecting the 2-D link of length  $R$  between the user and UAV-BS intersects the 3-D link between user and UAV-BS at the altitude of  $h_u$  if and only if this altitude is greater than  $h_b$  as in the figure.

## B. Blockages Process

The randomly positioned buildings are modeled using a Boolean scheme of random rectangles [17]. The blockage centers represented as  $C_k$  is a homogeneous PPP  $\Phi_b$  of intensity  $\lambda_b$ . By the definition of PPP, the blockages are placed independently of one another, ensuring the geometry of the blockages does not intersect. The lengths and widths of the blockages are assumed to be independent and identically distributed (i.i.d.), following the probability distributions  $f_L(l)$  and  $f_W(w)$ , respectively. The intensity, length, and width of the blockages are selected in such a way that the typical user moving in a straight line does not pass through the blockages. The probability of intersection between the user and the blockage is almost zero. Additionally, the orientation of the blockages,  $\theta_k$  is uniformly distributed over the interval  $(0, 2\pi]$ . The heights of the blockages are modeled by a Rayleigh distribution with probability density function (PDF)  $f_H(h)$  [18]. We observe the number of blockages  $N$  crossing the 2-D link between the user and the UAV-BS, which is a Poisson-distributed random variable. From Fig. 2,  $R$  represents the 2-D distance between the user and the UAV-BS.  $y$  indicates the distance from the user to the point where a building intersects the 2-D link of length  $R$ . Given that  $N$  buildings intersect the link, their intersection points are uniformly distributed along the interval  $[0, R]$  [17]. Thus,  $y$  is a random variable that follows a uniform distribution from  $[0, R]$  [37].

**Lemma 1.** *Given that a blockage intersects the 2-D link between the user and the UAV-BS of distance  $R$  at a height  $h_u$ , the conditional probability that it blocks the 3-D Euclidean link between the user and the UAV-BS is given as*

$$\mathbb{P}(h > h_b | y, h_u) = 1 - \int_0^{\frac{yh_u}{R}} f_H(h) dh, \quad (1)$$

where  $h_b = \frac{yh_u}{R}$ . Marginalizing over  $y$  and  $h_u$ ,

$$\eta = \frac{1}{(h_{max} - h_{min})} \int_{h_{min}}^{h_{max}} \int_0^1 \exp\left(-\frac{h^2 s^2}{2\sigma^2}\right) ds dh, \quad (2)$$

if and only if  $R > 0$ .

*Proof.* As mentioned above, the heights of the blockages are Rayleigh distributed with PDF given as  $f_H(x) = \frac{x}{\sigma^2} \exp\left(-\frac{x^2}{2\sigma^2}\right)$ . Leveraging the property of Rayleigh distribution, the average height of blockages  $H_b = 1.253\sigma$ .

The probability that the 3-D link is blocked is given as

$$\mathbb{P}(h > h_b | y, h_u) = 1 - \int_0^{\frac{yh_u}{R}} f_H(h) dh = \exp\left(-\frac{h_u^2 \left(\frac{y}{R}\right)^2}{2\sigma^2}\right). \quad (3)$$

Marginalizing (3) with respect  $y$ ,

$$\mathbb{P}(h > h_b | h_u) = \frac{1}{R} \int_0^R \exp\left(-\frac{h_u^2 \left(\frac{t}{R}\right)^2}{2\sigma^2}\right) dt. \quad (4)$$

Substituting  $\frac{t}{R} = s$ , and taking an expectation over  $h_u$ , uniformly distributed between  $h_{min}$  and  $h_{max}$ , we obtain (2).  $\square$

**Remark:** When  $R = 0$ , the UAV-BS is directly above the user. Substituting  $R = 0$  in (3), then the conditional probability  $\mathbb{P}(h > h_b | y, h_u) = 0$  holds. If we marginalize over  $y$  and  $h_u$ , the above un-conditioned probability  $\eta = 0$ . The total number of blockages crossing the 2-D link between the user and the UAV-BS is  $N$ . As the blockages are distributed as a PPP,  $N$  is a poisson random variable, and its mean is  $qR + p$ , where  $R$  is the length of the 2-D link [17].

$$\mathbb{E}[N] = qR + p \quad (5)$$

where  $q = \frac{2\lambda_b(\mathbb{E}[L_b] + \mathbb{E}[W_b])}{\pi}$  and  $p = \lambda_b \mathbb{E}[L_b] \mathbb{E}[W_b]$ , where  $\mathbb{E}[L_b]$  and  $\mathbb{E}[W_b]$  are evaluated by the average length and width of the blockages.  $\eta$  is independent on  $N$  as the intersections form PPP on the 2-D link of length  $R$ . Let  $\tilde{N}$  represent the number of blockages obstructing the 3-D link between the user and UAV-BS. By applying the independent thinning to  $N$ , the expected value of  $\mathbb{E}[\tilde{N}] = \eta \mathbb{E}[N]$ .

## C. Propagation Model

The UAV-BSs can either be in LoS or NLoS state [14] depending on visibility from the typical user. Let the locations of the LoS UAV-BSs be represented by  $\Phi_L$  and the locations of NLoS UAV-BSs be represented by  $\Phi_N$ . Therefore,  $\Phi_U = \Phi_L \cup \Phi_N$ . The LoS transmissions experience Nakagami distributed fast-fading,  $G_L$ , with parameter  $m$  [38]. The NLoS UAV-BS transmissions experience Rayleigh-distributed fast-fading  $g_N$ , with the variance equal to 1. The downlink transmit power of the UAV-BSs is  $P_u$ . For the large-scale path loss, we consider the received power at the typical user from the LoS UAV-BS which is at a distance of  $d_L$  is given by  $R_L = P_u K G_L d_L^{-\alpha_L}$  and the NLoS UAV-BS which is at a distance of  $d_N$  given as  $R_N = P_u K g_N d_N^{-\alpha_N}$ .  $\alpha_L$  is the pathloss exponent for LoS links and  $\alpha_N$  is the pathloss exponent for NLoS links. The probability of establishing an LoS connection between the UAV-BS at a distance of  $d$  and height  $h$  from the typical user is given as

$$L_S(d, h) = \exp\left(-\eta(q\sqrt{d^2 - h^2} + p)\right), \quad (6)$$

where  $h$  is the altitude of UAV-BS from the ground and  $d$  is the 3-D Euclidean distance between the UAV-BS and the user, according to the visibility state of the UAV-BS.

$$d = \begin{cases} d_L; & \alpha = \alpha_L \\ d_N; & \alpha = \alpha_N \end{cases} \quad (7)$$

Accordingly, the probability of NLoS transmissions is given as  $N_S(d, h) = 1 - L_S(d, h)$ . From (5), we observe the probability of establishing LoS link between the UAV-BS and the user is not only the function of the altitudes of UAV-BS and the Euclidean distance but also a function of the intensity of blockages, average length and width, and height of blockages.

## D. Performance Metrics

The main factors driving 5G technology are reliability and latency, which form the foundation of ultra-reliable low-latency communications (URLLC) and support applications requiring real-time responsiveness and consistent performance.

Considering this, we evaluate two critical performance metrics in a UAV network, where UAVs are modeled as a 2-D MPPP, by analyzing the coverage probability or success probability experienced by the user. The first metric involves a fine-grained analysis of the SINR experienced by the user, offering detailed insights into the reliability of communication links. This approach transcends traditional average SINR evaluations by capturing link-level variability considering CSP. The second metric addresses handover management, leveraging caching capabilities at the user terminal to reduce unnecessary HOs leading to latency and QoS degradation during mobility.

- **MD of SINR:** To perform a fine-grained analysis of SINR in a stationary and ergodic point process setting, we calculate MD of SINR. MD provides the distribution of the conditional success probability for a randomly selected user in a network. Unlike the mean SINR, which provides an average measure, the MD of SINR provides a probabilistic framework to analyze the reliability of communication links in a wireless network. It represents the complementary cumulative distribution function (CCDF) of the success probability  $\mathcal{P}_S(\gamma)$  conditioned on the point processes  $\Phi_U$  and  $\Phi_b$  [39].

$$\bar{F}_{\mathcal{P}_S}(\gamma, x_r) = \mathbb{P}^{\dagger}(\mathcal{P}_S(\gamma) > x_r), \quad \gamma \in \mathbb{R}^+, \quad x_r \in [0, 1], \quad (8)$$

where  $\mathbb{P}^{\dagger}$  represents the reduced Palm probability conditioning the typical user at the origin  $o$ ,  $x_r$  is the reliability threshold. The random variable  $\mathcal{P}_S(\gamma)$  is given as

$$\mathcal{P}_S(\gamma) = \mathbb{P}(\text{SINR} > \gamma | \Phi_U, \Phi_b). \quad (9)$$

- **Cache-enabled handover analysis:** The rate requirement for the services for the users is very important for a continuous and uninterrupted QoS. When the users are moving, it will lead to frequency handovers and handover failures, leading to degradation of this QoS. In a traditional cellular setup, handovers happen at every cell boundary, leading to excessive delay in communication. In order to reduce the latency experienced by the user due to handovers, we explore a novel HO management strategy aimed at minimizing handovers to provide a seamless user experience across applications such as autonomous driving, navigation, and video streaming. According to 3GPP standards [40], a user performs a cell search every  $t_s$  seconds. A handover is triggered when a neighboring UAV-BS offers a RSS higher than the associated UAV-BS. Each user requires  $\Delta T$  seconds to measure this RSS from the neighboring cell. We dynamically select  $t_s$  by leveraging caching capabilities in UE in motion. We consider every user to have a rate requirement of  $s_r$ , and every UE has a cache size of  $G$  and moving with a velocity of  $v$ . Initially, cache memory is empty. When the downloaded data by the user exceeds the required service rate  $s_r$ , the difference is stored in the cache. Using this cached data, the user can delay cell searches and avoid unnecessary HOs, thereby reducing latency and maintaining a high QoS during mobility.

To obtain the above metrics, we derive the distance distribution of the associated UAV-BS from the typical user and the SINR coverage probability experienced by the user.

### III. CHARACTERIZATION OF DISTANCE DISTRIBUTIONS AND ASSOCIATION PROBABILITIES

In this section, we obtain the distribution of the distance from a typical user to the nearest LoS or NLoS UAV-BS, where the locations of UAV-BSs are distributed as a 2-D MPPP.

**Lemma 2.** *Given that the typical user observes at least one LoS and one NLoS UAV-BS, the cumulative distribution function (CDF) for the distance distributions to the nearest LoS and NLoS UAV-BS distributed as a 2-D MPPP, defined as  $d_L$  and  $d_N$  respectively, are given as*

$$F_{d_L}(z) = \begin{cases} \left(1 - \exp\left(A \times \int_{h_{min}}^z \mathcal{L}(z, h) dh\right)\right) / B_L; & h_{min} \leq z < h_{max} \\ \left(1 - \exp\left(A \times \int_{h_{min}}^{h_{max}} \mathcal{L}(z, h) dh\right)\right) / B_L; & z \geq h_{max} \end{cases} \quad (10)$$

$$F_{d_N}(z) = \begin{cases} \left(1 - \exp\left(A \times \int_{h_{min}}^z \mathcal{N}(z, h) dh\right)\right); & h_{min} \leq z < h_{max} \\ \left(1 - \exp\left(A \times \int_{h_{min}}^{h_{max}} \mathcal{N}(z, h) dh\right)\right); & z \geq h_{max} \end{cases} \quad (11)$$

Here  $A = \frac{-2\lambda_u \pi}{(h_{max} - h_{min})}$  and  $\delta(z, h) = \sqrt{z^2 - h^2}$ , for  $R > 0$ .

$$\mathcal{L}(z, h) = \frac{\exp(-p\eta) - L_S(z, h)(q\eta\sqrt{z^2 - h^2} + 1)}{(q\eta)^2} \quad (12)$$

$$\mathcal{N}(z, h) = \frac{(z^2 - h^2)}{2} - \mathcal{L}(z, h) \quad (13)$$

*Proof.* See Appendix A.  $\square$

**Remark:** If  $R = 0$ , when the UAV is exactly above the user,  $L_S(z, h) = 1$ . In that case,  $\mathcal{L}(z, h) = \frac{(z^2 - h^2)}{2}$ ,  $\mathcal{N}(z, h) = 0$ .  $p$  and  $q$  are the functions of intensity and dimensions of blockages as defined in (5).  $B_L$  is the probability that there exists at least one LoS UAV-BS.

Based on the blockage process considered in this paper, in high-blockage scenarios, The probability of having at least one LoS UAV-BS is not guaranteed to be one. Therefore, from [41], we derive the expression for  $B_L$  given as

$$B_L = 1 - \exp\left(A \times \left[ \int_{h_{min}}^{h_{max}} \int_{h_{min}}^{z_1} \mathcal{L}(z_1, h_1) dh_1 dz_1 + \int_{h_{max}}^{\infty} \int_{h_{min}}^{h_{max}} \mathcal{L}(z_2, h_2) dh_2 dz_2 \right]\right). \quad (14)$$

However, given the blockage process, we observe that the probability of having at least one NLoS UAV-BS, considering they are distributed according to a PPP, is always one.

Taking the derivative of (10) and (11) with respect to  $z$ , the PDF of the distance of the typical user from the nearest LoS and NLoS UAV-BSs, given as,  $f_{d_L}(z)$  and  $f_{d_N}(z)$  respectively.

$$f_{d_L}(z) = \begin{cases} f'_{d_L}(z); & h_{min} \leq z < h_{max} \\ f_{d_L}(z); & z \geq h_{max} \end{cases} \quad (15)$$

Similar expressions are considered for  $f_{d_N}(z)$ .

Next, we derive the association probabilities for LoS and NLoS UAV-BSs. As previously mentioned, a typical user can connect to either a LoS or NLoS UAV-BS, depending on the maximum RSSI strategy.

**Lemma 3.** *The probability of association of the typical user with an NLoS UAV-BS,  $A_N$  is given by:*

$$A_N = \int_{h_{min}}^{h_{max}} \left[ \exp \left( A \times \int_{h_{min}}^{h_{max}} \mathcal{L}(r_1^{\frac{\alpha_N}{\alpha_L}}, h_a) dh_a \right) \right] f'_{d_N}(r_1) dr_1 + \int_{h_{max}}^{\infty} \left[ \exp \left( A \times \int_{h_{min}}^{h_{max}} \mathcal{L}(r_2^{\frac{\alpha_N}{\alpha_L}}, h_a) dh_a \right) \right] f''_{d_N}(r_2) dr_2 \quad (16)$$

where  $\mathcal{L}(z, h)$  is obtained from (12) and  $A = \frac{-2\lambda_u \pi}{(h_{max} - h_{min})}$ .

*Proof.* See Appendix B  $\square$

Naturally, the probability of LoS UAV-BS association  $A_L = 1 - A_N$ . This solution is valid when  $\alpha_N > \alpha_L$  and  $h_{min} \ll h_{max}$ , which is feasible in practical scenarios.

#### IV. META DISTRIBUTION OF SINR ANALYSIS

In this section, we derive the CSP experienced by the typical user associated with the LoS or NLoS UAV-BS, conditioned on the point processes  $\Phi_U$  and  $\Phi_b$ , to obtain the MD of SINR. Taking an expectation over the  $\Phi_U$  and  $\Phi_b$ , we calculate the  $b^{\text{th}}$  moment of the CSP. Without loss of generality, leveraging the ergodicity property of the PPP [34], we conduct the downlink analysis from the perspective of a typical user at the origin.

##### A. Conditional success probability of LoS UAV-BS

The coverage probability or conditional success probability  $P_{SL}(\gamma)$  experienced by the user associated to an LoS UAV-BS, conditioning on  $\Phi_U$  and  $\Phi_b$ , is given as

$$P_{SL}(\gamma) = \mathbb{P} \left( \frac{P_u K G_L d_L^{-\alpha_L}}{\sigma_N + I'_L + I_N} > \gamma | \Phi_U, \Phi_b \right), \quad (17)$$

where  $I'_L$  and  $I_N$  are the interfering strengths from the other LoS and NLoS UAV-BSs respectively, where  $I'_L = \sum_{i: X_i \in \Phi'_L} P_u K G'_L d_i^{-\alpha_L}$  and  $I_N = \sum_{i: X_i \in \Phi_N} P_u K g_N d_i^{-\alpha_N}$ .  $\Phi'_L$  is the point process of LoS UAV-BSs in which the associated LoS UAV-BS is omitted.

**Theorem 1.** *The  $b^{\text{th}}$  moment of  $P_{SL}(\gamma)$  is given as*

$$M_L(\gamma) = A_L \int_{h_{min}}^{h_{max}} \left[ A'(z) U'(z, \gamma, b) \times f_{d_L}(z) \right] dz + \int_{h_{max}}^{\infty} \left[ B'(z) U'(z, \gamma, b) \times f_{d_L}(z) \right] dz, \quad (18)$$

where

$$A'(z) = \exp \left( -2\pi\lambda_u l'_1(z) \right) \times \exp \left( -2\pi\lambda_u l'_2(z) \right). \quad (19)$$

$$B'(z) = \exp \left( -2\pi\lambda_u l'_3(z) \right) \times \exp \left( -2\pi\lambda_u l'_4(z) \right). \quad (20)$$

$$l'_1(z) = \int_0^{k(z)} \left( 1 - \left[ \int_{n(z,x)}^{h_{max}} \frac{\rho'(t,x)}{(h_{max} - n(z,x))} dt \right] \right) x dx + \int_{k(z)}^{\infty} \left( 1 - \left[ \int_{h_{min}}^{h_{max}} \frac{\rho'(t,x)}{(h_{max} - h_{min})} dt \right] \right) x dx. \quad (21)$$

$$l'_2(z) = \int_0^{k(z)} \left( 1 - \left[ \int_{n(z,x)}^{h_{max}} \frac{\tau'(t,x)}{(h_{max} - n(z,x))} dt \right] \right) x dx + \int_{k(z)}^{\infty} \left( 1 - \left[ \int_{h_{min}}^{h_{max}} \frac{\tau'(t,x)}{(h_{max} - h_{min})} dt \right] \right) x dx. \quad (22)$$

$$l'_3(z) = \int_{l(z)}^{k(z)} \left( 1 - \left[ \int_{n(z,x)}^{h_{max}} \frac{\rho'(t,x)}{(h_{max} - n(z,x))} dt \right] \right) x dx + \int_{k(z)}^{\infty} \left( 1 - \left[ \int_{h_{min}}^{h_{max}} \frac{\rho'(t,x)}{(h_{max} - h_{min})} dt \right] \right) x dx. \quad (23)$$

$$l'_4(z) = \int_{l(z)}^{k(z)} \left( 1 - \left[ \int_{n(z,x)}^{h_{max}} \frac{\tau'(t,x)}{(h_{max} - n(z,x))} dt \right] \right) x dx + \int_{k(z)}^{\infty} \left( 1 - \left[ \int_{h_{min}}^{h_{max}} \frac{\tau'(t,x)}{(h_{max} - h_{min})} dt \right] \right) x dx. \quad (24)$$

$$U'(z, \gamma, b) = \exp \left( \frac{-\gamma \sigma_N b}{P_u K z^{-\alpha_L}} \right), \quad k(z) = \sqrt{z^2 - h_{min}^2}, \\ n(z, x) = \sqrt{z^2 - x^2}, \quad l(z) = \sqrt{z^2 - h_{max}^2}.$$

$$\rho'(t, x) = L_S(\sqrt{x^2 + t^2}, t) \left( \frac{1}{1 + \frac{\gamma(\sqrt{x^2 + t^2})^{-\alpha_L}}{z^{-\alpha_L}}} \right)^b + N_S(\sqrt{x^2 + t^2}, t) \left( \frac{1}{1 + \frac{\gamma(\sqrt{x^2 + t^2})^{-\alpha_N}}{z^{-\alpha_L}}} \right)^b. \quad (25)$$

$$\tau'(t, x) = L_S(\sqrt{x^2 + t^2}, t) \left( \frac{m}{m + \frac{\varepsilon \gamma(\sqrt{x^2 + t^2})^{-\alpha_L}}{z^{-\alpha_L}}} \right)^{mb} + N_S(\sqrt{x^2 + t^2}, t) \left( \frac{m}{m + \frac{\varepsilon \gamma(\sqrt{x^2 + t^2})^{-\alpha_N}}{z^{-\alpha_L}}} \right)^{mb}. \quad (26)$$

where  $\varepsilon = m(m!)^{\frac{-1}{m}}$ .

*Proof.* See Appendix C.  $\square$

### B. Conditional success probability of NLoS UAV-BS

Here, we derive the conditional success probability  $P_{SN}(\gamma)$  of the typical user associated to an NLoS UAV-BS, i.e.,

$$P_{SN}(\gamma) = \mathbb{P}\left(\frac{P_u K g_N d_N^{-\alpha_N}}{\sigma_N + I'_N + I_L} > \gamma | \Phi_U, \Phi_b\right), \quad (27)$$

where  $I_L$  and  $I'_N$  are the interfering strengths from the LoS and the other NLoS UAV-BSs respectively, where  $I_L = \sum_{i: \mathbf{x}_i \in \Phi_L} P_u K G_L d_L^{-\alpha_L}$  and  $I_N = \sum_{i: \mathbf{x}_i \in \Phi'_N} P_u K g'_N d_N^{-\alpha_N}$ .  $\Phi'_N$  is the point process of NLoS UAV-BSs in which the associated NLoS UAV-BS is omitted.

**Theorem 2.** *The  $b^{th}$  moment of  $P_{SN}(\gamma)$  is given as*

$$M_N(\gamma) = A_N \int_{h_{min}}^{h_{max}} \left[ A''(z) U''(z, \gamma, b) \times f_{d_N}(z) \right] dz + \int_{h_{max}}^{\infty} \left[ B''(z) U''(z, \gamma, b) \times f_{d_N}(z) \right] dz, \quad (28)$$

where

$$A''(z) = \exp\left(-2\pi\lambda_u l_1''(z)\right) \times \exp\left(-2\pi\lambda_u l_2''(z)\right). \quad (29)$$

$$B''(z) = \exp\left(-2\pi\lambda_u l_3''(z)\right) \times \exp\left(-2\pi\lambda_u l_4''(z)\right). \quad (30)$$

$$l_1''(z) = \int_0^{k(z)} \left( 1 - \left[ \int_{n(z,x)}^{h_{max}} \frac{\rho''(t,x)}{(h_{max} - n(z,x))} dt \right] \right) dx + \int_{k(z)}^{\infty} \left( 1 - \left[ \int_{h_{min}}^{h_{max}} \frac{\rho''(t,x)}{(h_{max} - h_{min})} dt \right] \right) dx. \quad (31)$$

$$l_2''(z) = \int_0^{k(z)} \left( 1 - \left[ \int_{n(z,x)}^{h_{max}} \frac{\tau''(t,x)}{(h_{max} - n(z,x))} dt \right] \right) dx + \int_{k(z)}^{\infty} \left( 1 - \left[ \int_{h_{min}}^{h_{max}} \frac{\tau''(t,x)}{(h_{max} - h_{min})} dt \right] \right) dx. \quad (32)$$

$$l_3''(z) = \int_{l(z)}^{k(z)} \left( 1 - \left[ \int_{n(z,x)}^{h_{max}} \frac{\rho''(t,x)}{(h_{max} - n(z,x))} dt \right] \right) dx + \int_{k(z)}^{\infty} \left( 1 - \left[ \int_{h_{min}}^{h_{max}} \frac{\rho''(t,x)}{(h_{max} - h_{min})} dt \right] \right) dx. \quad (33)$$

$$l_4''(z) = \int_{l(z)}^{k(z)} \left( 1 - \left[ \int_{n(z,x)}^{h_{max}} \frac{\tau''(t,x)}{(h_{max} - n(z,x))} dt \right] \right) dx + \int_{k(z)}^{\infty} \left( 1 - \left[ \int_{h_{min}}^{h_{max}} \frac{\tau''(t,x)}{(h_{max} - h_{min})} dt \right] \right) dx. \quad (34)$$

$$U'(z, \gamma, b) = \exp\left(\frac{-\gamma \sigma_N b}{P_u K z^{-\alpha_N}}\right), \quad k(z) = \sqrt{z^2 - h_{min}^2}, \\ n(z, x) = \sqrt{z^2 - x^2}, \quad l(z) = \sqrt{z^2 - h_{max}^2}.$$

$$\rho''(t, x) = L_S(\sqrt{x^2 + t^2}, t) \left( \frac{1}{1 + \frac{\gamma(\sqrt{x^2 + t^2})^{-\alpha_L}}{z^{-\alpha_N}}} \right)^b + N_S(\sqrt{x^2 + t^2}, t) \left( \frac{1}{1 + \frac{\gamma(\sqrt{x^2 + t^2})^{-\alpha_N}}{z^{-\alpha_N}}} \right)^b. \quad (35)$$

$$\tau''(t, x) = L_S(\sqrt{x^2 + t^2}, t) \left( \frac{m}{m + \frac{\varepsilon \gamma (\sqrt{x^2 + t^2})^{-\alpha_L}}{z^{-\alpha_N}}} \right)^{mb} + N_S(\sqrt{x^2 + t^2}, t) \left( \frac{m}{m + \frac{\varepsilon \gamma (\sqrt{x^2 + t^2})^{-\alpha_N}}{z^{-\alpha_N}}} \right)^{mb}. \quad (36)$$

The proof is the same as Theorem 1; therefore, we skip it for brevity.

The MD of SINR provides a probabilistic framework to analyze the reliability of communication links in a wireless network. For an ergodic point process in UAV networks, the MD  $\bar{F}_{P_S}(\gamma, x_r)$  can be interpreted as the proportion of active links where the success probability  $\mathcal{P}_S(\gamma)$  for a given value of threshold  $\gamma$  exceeds the reliability threshold  $x_r$ . The exact MD can be obtained from the Gil-Pelaez theorem [42] with  $b^{th}$  moment  $M_b$  of  $\mathcal{P}_S(\gamma)$ ,  $b \in \mathbb{R}$ ,  $i = \sqrt{-1}$ .

$$\bar{F}_{P_S}(\gamma, x_r) = \frac{1}{2} + \frac{1}{\pi} \int_0^{\infty} \frac{\Im(e^{-it \log x_r} M_{it})}{t} dt, \quad (37)$$

where  $\Im(z)$  is the imaginary part of  $z \in \mathbb{C}$ .  $M_{it}$  is the  $it^{th}$  moment of  $\mathcal{P}_S(\gamma)$ .

From (18) and (28), the  $b^{th}$  moment of the  $\mathcal{P}_S(\gamma)$  given as

$$M_b(\gamma) = A_L M_L(\gamma) + A_N M_N(\gamma). \quad (38)$$

The SINR MD is obtained by substituting (38) in (37).

The first moment of  $\mathcal{P}_S(\gamma)$ , substituting  $b = 1$  in (38), gives the overall SINR coverage probability experienced by the user. The  $(-1)^{th}$  moment of  $\mathcal{P}_S(\gamma)$  is referred to as mean local delay (MLD)  $M_{-1}(\gamma)$ , represents the average number of retransmission attempts required to successfully transmit a packet between the UAV-BS and the user.

## V. CACHE-ENABLED HO ANALYSIS

In this section, we discuss an efficient HO management scheme by leveraging the caching capabilities of the UE. In our work in [32], we discuss HO management using caching in a 1-D network and analyze the impact of handovers on network performance and delay. Here, we extend this to a UAV-based network, with locations of UAVs modeled as a 2-D MPPP, in the presence of blockages. This HO management scheme reduces handovers in the network, thus reducing the latency in transmission in the presence of mobile users. We perform a semi-analytical analysis of the network to derive the average throughput experienced by the user in a cache-enabled HO scheme. Without loss of generality, we perform a downlink analysis from the perspective of a mobile user moving in a straight line through the origin along the x-axis.

We consider a scenario where a user moves over a long period, denoted as  $T$ . At  $t = 0$ , the user will be associated with a UAV-BS at  $(x_a, y_a, h_a)$  and experience a download rate of  $d_r(t)$ . The download rate experienced by the user associated with an LoS UAV-BS at time  $t$  is given as

$$d_r(t) = B \log_2 \left( 1 + \frac{P_u K G_L d_{mu}(t)^{-\alpha_L}}{\sigma_N + I'_L + I_N} \right), \quad (39)$$

where  $I'_L$  and  $I_N$  are the interfering strengths from the other LoS and NLoS UAV-BSs respectively.  $d_{mu}(t)$  is the distance between the associated BS and the user at time  $t$ , given as  $d_{mu}(t) = \sqrt{(x_a - vt)^2 + (y_a - y_u)^2 + h_a^2}$ .

We assume the user is moving along the 2-D plane in a straight line with velocity  $v$ .  $G_L$  is the Nakagami-m fading factor,  $K$  is the pathloss coefficient i.e.,  $K = (\frac{\lambda_c}{4\pi})^2$ , where  $\lambda_c$  is the carrier wavelength. If it is NLoS UAV-BS, the pathloss and fading parameters change.

Consider the scenario where  $d_r > s_r$ . As the user moves forward, the user experiences a download rate greater than  $s_r$ . Consequently, the excess data (i.e., the difference between the downloaded data and the required data for the service) is cached in the UE memory of cache size  $G$ . The caching continues as long as the user's download rate is equal to or exceeds the required service rate and there is available space in the cache. Let  $t_d$  represent the time at which the download rate falls below the service's required rate. This time, referred to as the caching time, marks when caching occurs at the UE, given the download rate  $d_r$  is greater than  $s_r$ . In the presence of blockages, this time is discontinuous, making its analytical expression intractable. The downloaded data till time  $t_d$  is given as  $C_D = \int_0^{t_d} d_r(t) dt$ .

The amount of data used by the user to meet the service requirement till time  $t_n$  is given as  $s_r t_n$ . The user requires  $\Delta T$  seconds to measure the RSSI from the neighboring cells. If there is sufficient data cached, i.e., more than  $s_r \Delta T$ , to skip HOs and perform RSS measurements, the cell search is muted, and HOs are skipped. The user remains associated with the previous UAV-BS until the next cell search is initiated. While utilizing cached data  $C_D$ , the user achieves the specified service rate  $s_r$ . Let the time be  $t_n$ , which the user can use the cached data to maintain the service requirement rate. If there is  $C_D$  data in the cache, the next cell search is triggered when the condition  $C_D/s_r < \Delta T$  is met. The user maintains association with the current UAV-BS until this condition is satisfied or the download rate falls below the minimum threshold defined by 3GPP to sustain a connection. Once this occurs, the service rate drops to the current download rate  $d_r(t)$ , prompting a cell search, RSS measurements, and the initiation of a handover. Using this methodology, the number of handovers experienced by the user in the cache-enabled HO scheme is given as  $H_N$ . By performing temporal and spatial averaging, the average HO rate is given as  $\mu = \frac{H_N}{T}$ . Performing spatial averaging, the average HO rate is given as  $\mu'$ . The throughput experienced by the user when utilizing the cached data is  $s_r$ . Considering the entire time of travel  $T$ , the average throughput at the time of utilizing cached data is given as  $\frac{s_r t_n}{T}$ . Performing spatial averaging, the average throughput experienced by the user when utilizing the cached data is given as  $R_s$ . While the user experiences the download rate  $d_r$  less than the service rate, we derive the average throughput by utilizing the first moment of CSP  $M_1(\gamma)$  derived in (38).

$$R_d = B \int_0^{2^{\frac{s_r}{B}} - 1} \frac{M_1(k)}{k+1} dk. \quad (40)$$

Here, the maximum SINR experienced by the user will be  $2^{\frac{s_r}{B}} - 1$ , which is the SINR experienced by the user when the cached data is fully exhausted before initiating the cell search.

Therefore, the overall average throughput experienced by the user is given as  $R'_a = R_s + R_b$ .

### A. Effective Average Rate

The effective average throughput experienced by the user is given as [32]

$$R_{\text{eff}} = R'_a (1 - \mu' t_H)^+, \quad (41)$$

where  $\mu'$  is the average handover rate. The time overhead for each handover  $t_H$  is 43 ms [43]. The delay experienced by the user due to the HOs is expressed as  $\mu' t_H$ .

## VI. NUMERICAL RESULTS AND DISCUSSIONS

In this section, we validate the theoretical model through Monte Carlo simulations and provide numerical results to discuss the key characteristics of the network. The parameters are  $P_u = 10$  W [23],  $h_{\min} = 100$  m,  $h_{\max} = 300$  m,  $B = 100$  MHz [44],  $\alpha_L = 2$ ,  $\alpha_N = 4$ ,  $v = 1$  m/s,  $f_c = 3.5$  GHz,  $\lambda_b = 10^{-6}$  km<sup>-2</sup>,  $s_r = 40$  Mbps,  $t_H = 43$  ms,  $T = 5000$  s,  $t_s = 20$  ms.

In Fig. 3, we plot the SINR MD as a function of the intensity of UAV-BSs across various blockage scenarios, with a reliability threshold of  $x_r = 0.9$ , indicating that 90% of the communication links are active. In low-blockage scenarios, for an intensity of  $\lambda_u = 10^{-6}$ , the SINR MD value is 0.7. This implies that the probability of achieving the reliability threshold, where 90% of the communication links between the user and the UAV-BSs are active, is 70%. However, in scenarios with higher blockages, users achieve the reliability threshold of 90% active links less than 55% of the time. Contrary to popular belief, regions with higher blockages benefit from a denser deployment of UAV-BSs, as the blockages help reduce interference from other UAV-BSs. We also observe that increasing the network density does not improve performance beyond a certain limit. In Fig. 4, we plot the SINR MD as a function of the intensity of UAV-BSs, evaluated at a reliability threshold of 0.05. This threshold signifies that at least 5% of the communication links are active, with the SINR exceeding a specified value. The results reveal that areas with lower blockage require fewer UAV-BSs to sustain this level of active communication links, whereas higher blockage areas demand a denser deployment. In low-blockage scenarios where  $\lambda_b = 10^{-6}$ , users consistently experience at least 5% of active communication links. In contrast, in high-blockage scenarios  $\lambda_b = 10^{-2}$ , increasing the density of UAV-BSs beyond 10 UAV-BSs per km<sup>2</sup> ensures that all users achieve at least 5% of active communication links at all times.

In Fig. 5, we plot MLD in the network for different values of SINR requirement at the users. Here, we observe for a fixed value of UAV-BS intensity of  $10^{-5}$ , the increase in blockage intensity leads to an increase in SINR threshold  $\gamma$  because in order to maintain a consistent mean local delay while ensuring SINR constraints are met, the system must increase the SINR threshold. However, for fixed blockage intensity of  $10^{-5}$ , an increase in UAV-BS intensity leads to a decrease in  $\gamma$ . This is because the user can experience the required communication quality more easily due to better coverage. Fig. 6 shows the LoS association probability of the network versus the intensity of UAV-BSs. As the intensity of UAV-BSs increases, LoS association probability decreases. For sparse deployment of UAV-BSs, LoS association is high and



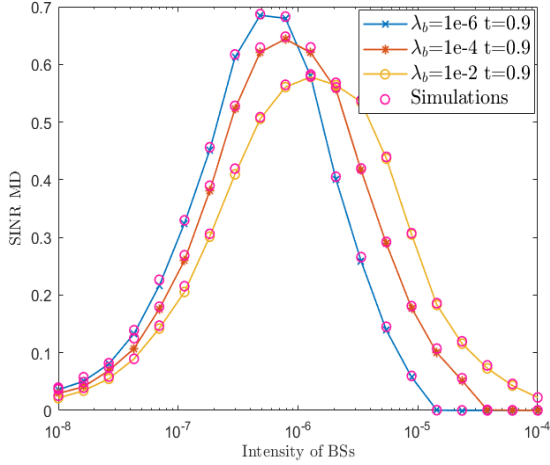


Fig. 3. SINR MD as a function of the intensity of UAV-BSs for different blockage intensities for  $x_r = 0.9$ ,  $\gamma = -10$  dB

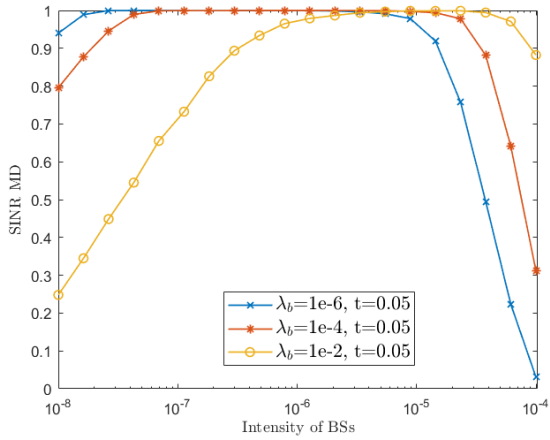


Fig. 4. SINR MD as a function of the intensity of UAV-BSs for different blockage intensities for  $x_r = 0.05$ ,  $\gamma = 10$  dB

then decreases as the intensity of UAV-BSs increases. In the presence of TBSs as discussed in [14], LoS associations are fewer for lower values of intensity of BSs. Further increasing the intensity of UAV-BSs enhances the likelihood of serving NLoS UAV-BSs without significantly impacting the LoS links. Here, we discuss the LoS association trend in the absence of TBSs. The key insight is that network densification alone is not an effective solution for increasing the LoS association probability or enhancing the network's coverage performance. Intuitively, as blockages increase, the probability of LoS association decreases. However, a higher density of NLoS UAV-BSs can mitigate interference, leading to an improvement in SINR, as discussed in Fig. 3 and Fig. 4.

In Fig. 7, we observe that as the SINR threshold increases, the CSP decreases. For a given blockage intensity, increasing the deployment density of UAV-BSs degrades network performance due to an increase in interference. Furthermore, when user requirements are low, blockages do not significantly impact network performance, as they help block interference. However, when user requirements are high, blockages have a negative effect on performance by reducing LoS connections,

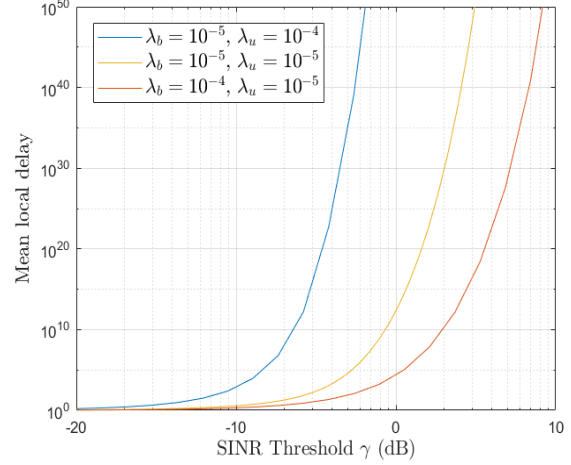


Fig. 5. Mean local delay versus SINR threshold

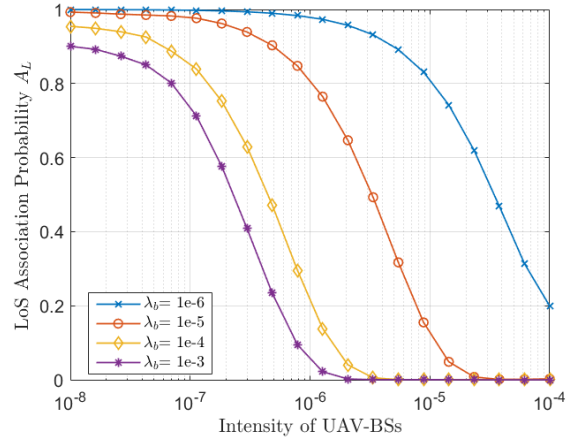


Fig. 6. LoS Association Probabilities for different blockage intensities

thereby impairing network reliability. In Fig. 8, we plot CSP versus intensity of UAV-BSs for different blockage intensities and minimum altitude of the UAV-BSs. As discussed, in denser deployments, higher blockage scenarios offer better performance because of the blocking of the signals interfering UAV-BSs. Additionally, we observe that in areas with fewer blockages, deploying UAV-BSs at lower altitudes enhances performance by increasing LoS connections. In contrast, for areas with higher blockage intensity, deploying UAV-BSs at higher altitudes improves performance by establishing more LoS links, which is critical in overcoming the effects of large blockages.

Fig. 9 shows the HO delay is analyzed with respect to the intensity of UAV-BSs for various handover strategies. The conventional HO scheme exhibits higher handover rates compared to the cache-based scheme, as the latter bypasses unnecessary handovers by leveraging cached data at the UE. The cache-based strategy avoids initiating new associations when the cached data at the UE is utilized, even in the presence of blockages. This reduces the overall handover delay in the network, thereby decreasing latency. However, if we increase the intensity of UAV-BSs after a certain limit, the

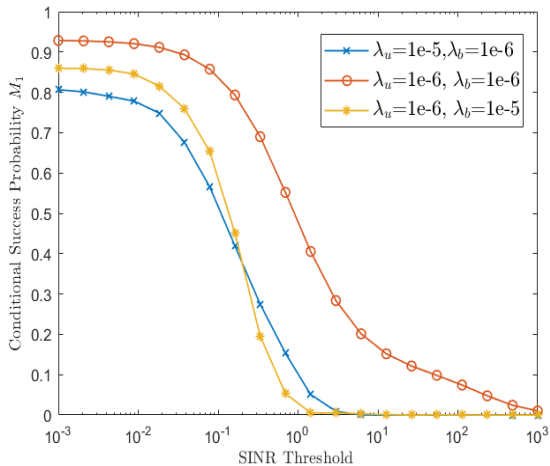


Fig. 7. Conditional success probability versus SINR threshold  $\gamma$

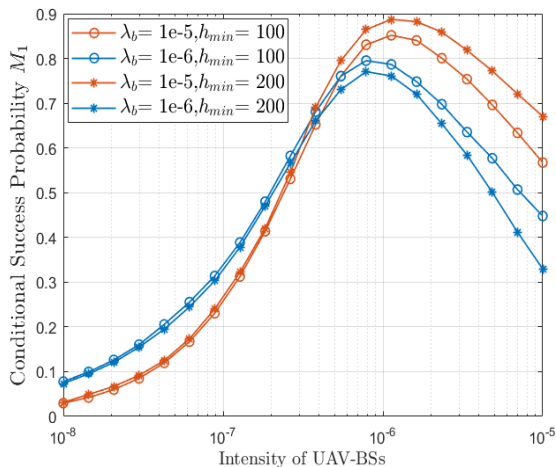


Fig. 8. Conditional success probability of the network versus the intensity of UAV-BSs for different blockage intensities and UAV altitudes with  $h_{max} = 300$  m,  $\gamma = -10$  dB

cache-based scheme results in the same HO delay as the conventional because of the decrease in the cache data at the UE end. This reduction occurs because increased BS density leads to higher interference, lowering the user's download rate and, consequently, reducing the cached data. In Fig. 10, we plot the average throughput experienced by the UE versus the intensity of UAV-BSs. We observe that the cache-based scheme provides better performance compared to the conventional scheme. For sparse deployment of BSs, both the cache-based and conventional schemes are negatively affected by blockages. However, for dense deployments of UAV-BSs, blockages block the interference, thus improving the network performance. Nevertheless, after reaching a certain UAV-BS deployment density, the average throughput for the cache-based scheme converges with that of the conventional scheme due to increased interference, leading to a depletion of the cached data.

In Fig. 11, we illustrate the variation in the energy efficiency of the system as the intensity of UAV-BSs increases, comparing conventional and cache-enabled handover (HO)

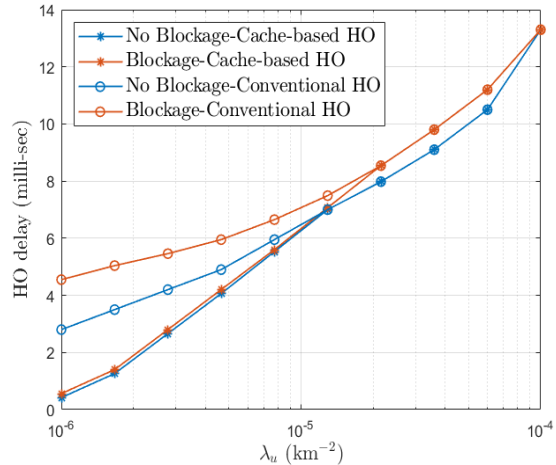


Fig. 9. Handover Delay versus Intensity of UAV-BS with  $s_r = 40$  Mbps,  $\lambda_b = 10^{-6}$  km $^{-2}$

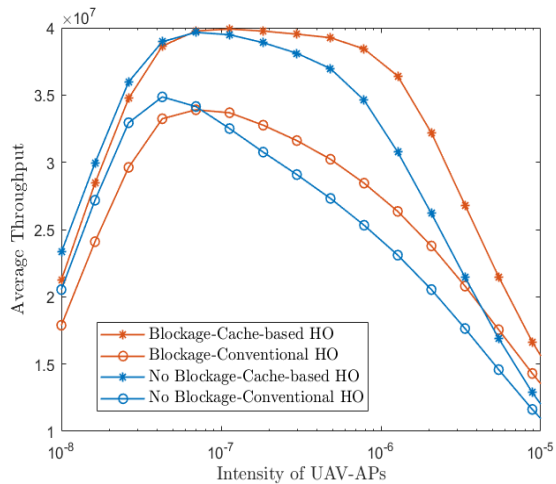


Fig. 10. Effective Average Throughput versus Intensity of UAV-BS with  $s_r = 40$  Mbps,  $\lambda_b = 10^{-6}$  km $^{-2}$ .

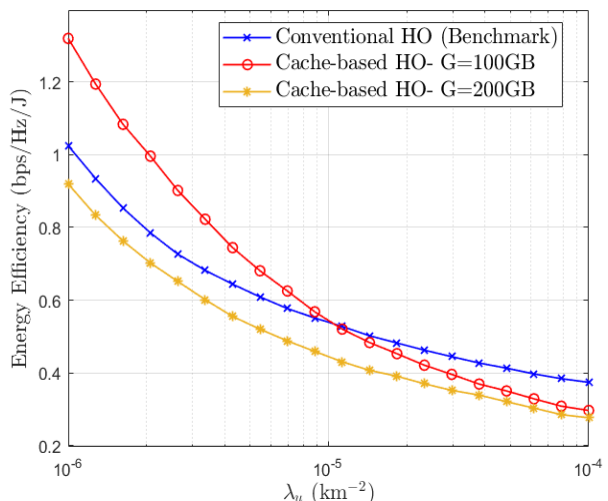


Fig. 11. Energy Efficiency versus Intensity of UAV-BSs with  $\lambda_b = 10^{-6}$  km $^{-2}$ ,  $s_r = 40$  Mbps

schemes. The same power consumption model as in our previous work [32] is adopted. For a caching capacity of 100 GB, the cache-enabled HO scheme outperforms the conventional scheme up to a UAV-BS intensity of approximately 10 UAV-BSs per  $km^2$ . This is due to the higher spectral efficiency and reduced inter-frequency HOs achieved through caching, even when accounting for the power consumption due to caching. However, as the UAV-BS intensity increases further, higher interference levels result in a decline in spectral efficiency and an increase in the HO rate, ultimately reducing energy efficiency. For a larger cache size of 200 GB, due to the power consumption associated with caching, the cache-enabled scheme performs worse than the conventional scheme in terms of energy efficiency.

## VII. CONCLUSION

In this work, we studied a UAV-based network designed to meet the service rate requirements of mobile users in the presence of urban blockages. Using stochastic geometry, we modeled the network to derive the distance distribution and association probabilities for the nearest LoS and NLoS UAV-BSs. We observed increasing network density does not necessarily enhance LoS associations, and blockages can improve network reliability by reducing interference. We analyze the MD of SINR to evaluate the network's reliability under various blockage scenarios. Additionally, we proposed a cache-enabled HO management scheme that leverages caching at user equipment to minimize unnecessary handovers, reduce latency, and improve throughput. A complete analytical framework for the same will be addressed in the future.

### APPENDIX A PROOF OF LEMMA 2

The heights of the UAVs are uniformly distributed from  $h_{min}$  and  $h_{max}$ .  $d_L$  and  $d_N$  are the 3-D Euclidean distance of the nearest LoS and NLoS UAV-BSs from the typical user, respectively. The cdf of  $d_L$  between the typical user and nearest LoS UAV-BS is given as

$$F_{d_L}(z) = \mathbb{P}(d_L \leq z) = 1 - \mathbb{P}(d_L > z) \quad (42)$$

The two cases are: (i)  $h_{min} \leq d_L < h_{max}$  (ii)  $d_L \geq h_{max}$ .

For case 1, we consider  $h_{min} \leq d_L < h_{max}$ , hence the heights of the UAV-BS is constrained to  $[h_{min}, d_L]$ . Consequently, we consider exclusively on those UAV-BSs whose heights fall within this specified range, leading to the formulation of a thinned PPP. The intensity of thinned PPP is given as  $\lambda_u \frac{d_L - h_{min}}{h_{max} - h_{min}}$ , since the heights of UAV-BSs are uniformly distributed from  $h_{min}$  to  $h_{max}$ . This models the spatial distribution of UAV-BSs within the specified height constraints. The 3-D Euclidean distance  $d_L$  is represented as 2-D distance  $r_L$  and height  $h_L$ , where  $d_L = \sqrt{r^2 + h^2}$ . Given that a UAV-BS is located at a 3-D distance  $d_L$  and height  $h$ , the probability that this UAV-BS is in line-of-sight (LoS) is denoted by  $L_S(d_L, h)$ . To determine the total probability of LoS with respect to the 2-D distance  $r$  between the user and the UAV-BS, the analysis requires integrating the dimensions of  $L_S(\sqrt{r^2 + h^2}, h)$  over the polar coordinates  $r$

and  $\theta$  covering a circular region of radius  $r$ . This gives the 2-D area where the probability of a UAV-BS being in LoS is taken into account within the circular region. To account for the variations in  $h$ , which is uniformly distributed from  $h_{min}$  to  $h_{max}$ , an expectation over  $h$  is taken. This provides the effective area within the 3-D space where there is a possibility of the UAV-BS being in LoS from the user. This quantifies the spatial region in which LoS conditions are likely to be met, considering both the 2-D distribution of locations of UAV-BSs and their random heights.

Applying the proper limits for  $r$ ,  $h$  and  $\theta$ , the void probability is given as

$$\mathcal{V}(d_L) = \exp \left( -2\pi\lambda_u \frac{(d_L - h_{min})}{(h_{max} - h_{min})} \int_{h_{min}}^{d_L} \frac{1}{(d_L - h_{min})} \int_0^{\delta(d_L, h)} L_S(\sqrt{r^2 + h^2}, h) r dr dh \right) \quad (43)$$

where  $\delta(d_L, h) = \sqrt{d_L^2 - h^2}$ . The inner integral can be represented as  $\mathcal{L}(d_L, h) = \int_0^{\delta(d_L, h)} L_S(\sqrt{r^2 + h^2}, h) r dr$ .

Therefore, the CDF is given as  $F_{d_L}(z) = (1 - \mathcal{V}(z)) / B_L$ .

$B_L$  is the probability that there is at least one LoS UAV-BS given in (14). The derivation follows the same as in [41].

For case 2, where  $d_L$  is greater than or equal to  $h_{max}$ , the heights of UAV-BSs can be anywhere between  $h_{min}$  and  $h_{max}$ . Given that the altitudes of the UAVs are uniformly distributed from  $h_{min}$  to  $h_{max}$ ,  $\mathbb{P}(h_{min} \leq h \leq h_{max}) = 1$ . Consequently, the entire spatial distribution of UAV-BS within the height of  $h_{min}$  to  $h_{max}$  are considered. By calculating the effective area where there is a possibility of being in LoS from the user, considering the 2-D locations and random heights, the CDF  $F_{d_N}(z)$  can be represented as

$$F_{d_N}(z) = \left[ 1 - \exp \left( -2\pi\lambda_u \int_{h_{min}}^{h_{max}} \frac{1}{(h_{max} - h_{min})} \int_0^{\delta(z, h)} L_S(\sqrt{r^2 + h^2}, h) r dr dh \right) \right] / B_L \quad (44)$$

Similarly, the distance distribution of nearest NLoS UAV-BS  $F_{d_N}(z)$  can be derived. If  $R = 0$ , then  $\eta = 0$ , and the inner integral  $\int_0^{\delta(z, h)} L_S(\sqrt{r^2 + h^2}, h) r dr dh = \frac{(z^2 - h^2)}{2}$ .

### APPENDIX B PROOF OF LEMMA 3

The probability of associating to an NLoS UAV-BS can be derived as

$$\mathbb{P}(P_u d_N^{-\alpha_N} > P_u d_L^{-\alpha_L}) = \mathbb{P}(d_L > d_N^{\frac{\alpha_N}{\alpha_L}}) \quad (45)$$

The event in which there is at least one LoS UAV-BS is given as  $E_1$ . The event that there are no LoS UAV-BSs is given as  $E_2$ . The event that there is atleast one NLoS UAV-BSs is given as  $E_3$ . Based on our blockage model,  $\mathbb{P}(E_3) = 1$ .

The probability that the other events occur is given below: (i)  $\mathbb{P}(E_1) = B_L$  (ii)  $\mathbb{P}(E_2) = (1 - B_L)$ .  $B_L$  is given in (14).

Therefore, the user getting associated with an NLoS UAV-BS can occur in two possible scenarios:

- The joint probability of having no LoS UAV-BS and at least one NLoS UAV-BS, the probability of associating to NLoS UAV-BS is given as  $\mathbb{P}(E_3)\mathbb{P}(E_2)$ .
- The joint probability of having at least one LoS UAV-BS and at least one NLoS UAV-BS, and under those conditions, the probability of associating to NLoS UAV-BS is given as

$$\mathbb{P}(E_3)\mathbb{P}(E_1)\left[\mathbb{P}(d_L > d_N^{\frac{\alpha_N}{\alpha_L}} | E_3, E_1)\right] \quad (46)$$

The probability of associating to an NLoS UAV-BS for scenario 1 is given as  $A_N^1 = (1 - B_L)$ .

For scenario 2, we apply the CCDF for  $d_L$  from (10) and take an expectation over  $d_N$ .

We know the path loss in NLoS links is much higher than that of LoS links. Therefore,  $\alpha_N \gg \alpha_L$ . The distance to the nearest NLoS UAV-BS  $d_N$  varies from  $h_{min}$  to  $\infty$ . Therefore, the values of  $d_L$  are always greater than  $h_{max}$ . Hence, the height of LoS UAV-BS always vary from  $h_{min}$  to  $h_{max}$ , since  $\alpha_N$  is greater than  $\alpha_L$ .

Given that there exists at least one LoS UAV-BS and one NLoS UAV-BS, the distance to the LoS UAV-BS  $d_L$  is greater than  $d_N^{\frac{\alpha_N}{\alpha_L}}$  if and only if there are no LoS UAV-BSs inside the

3-D region  $\mathcal{B}$  with radius  $\sqrt{d_N^{\frac{2\alpha_N}{\alpha_L}} - h_a^2}$  and height  $h_a$ .

Therefore, taking the CCDF of  $d_L$  from (10).

$$\mathbb{P}(d_L > d_N^{\frac{\alpha_N}{\alpha_L}} | E_3, E_1) = 1 - F_{d_L}(d_N^{\frac{\alpha_N}{\alpha_L}}) \quad (47)$$

$$\frac{\left[\exp\left(A \times \int_{h_{min}}^{h_{max}} \mathcal{L}(d_N^{\frac{\alpha_N}{\alpha_L}}, h_a) dh_a\right) - (1 - B_L)\right]}{B_L} \quad (48)$$

where  $A = \frac{-2\lambda_u\pi}{(h_{max} - h_{min})}$ ,  $\mathcal{L}(z, h)$  is given in (12).

Therefore, the probability of associating to an NLoS UAV-BS for scenario 2 is given as

$$A_N^2(d_N) = B_L \frac{\left[\exp\left(A \times \int_{h_{min}}^{h_{max}} \mathcal{L}(d_N^{\frac{\alpha_N}{\alpha_L}}, h_a) dh_a\right) - (1 - B_L)\right]}{B_L} \quad (49)$$

Combining both scenarios, the probability of associating with an NLoS UAV-BS is given as

$$A'_N(d_N) = A_N^1 + A_N^2(d_N) \quad (50)$$

$$A'_N(d_N) = (1 - B_L) + \exp\left(A \times \int_{h_{min}}^{h_{max}} \mathcal{L}(d_N^{\frac{\alpha_N}{\alpha_L}}, h_a) dh_a\right) - 1 + B_L \quad (51)$$

$$= \exp\left(A \times \int_{h_{min}}^{h_{max}} \mathcal{L}(d_N^{\frac{\alpha_N}{\alpha_L}}, h_a) dh_a\right) \quad (52)$$

Further, taking an expectation over  $d_N$ ,

$$A_N = \int_{h_{min}}^{h_{max}} \left[\exp\left(A \times \int_{h_{min}}^{h_{max}} \mathcal{L}(r_1^{\frac{\alpha_N}{\alpha_L}}, h_a) dh_a\right)\right] f'_{d_N}(r_1) dr_1 + \int_{h_{max}}^{\infty} \left[\exp\left(A \times \int_{h_{min}}^{h_{max}} \mathcal{L}(r_2^{\frac{\alpha_N}{\alpha_L}}, h_a) dh_a\right)\right] f''_{d_N}(r_2) dr_2 \quad (53)$$

where  $f'_{d_N}(r_1)$  and  $f''_{d_N}(r_2)$  are the derivative of CDF at (11).

## APPENDIX C PROOF OF THEOREM 1

The conditional success probability of associating to an LoS UAV-BS is given as

$$P_{SL}(\gamma) = \mathbb{P}\left(\frac{P_u K g_l d_L^{-\alpha_L}}{\sigma_N + I'_L + I_N} > \gamma | \Phi_U, \Phi_b\right) \quad (54)$$

where  $I'_L$  and  $I_N$  are the interfering strengths from the other LoS and NLoS UAV-BSs respectively, where  $I'_L = \sum_{i: \mathbf{X}_i \in \Phi'_L} P_u K G'_L d_L'^{-\alpha_L}$  and  $I_N = \sum_{i: \mathbf{X}_i \in \Phi_N} P_u K G_N d_N^{-\alpha_N}$ .

Conditioning on  $\Phi_U$  and  $\Phi_b$ , we apply the CCDF of the exponentially random variable  $g_l$  and take the expectation over  $g'_l$ .

$$P'_{SL}(\gamma) = \exp\left(\frac{-\gamma\sigma_N}{P_u K d_L^{-\alpha_L}}\right) \prod_{i: \mathbf{X}_i \in \Phi_N} \left(\frac{1}{1 + \frac{\gamma d_N^{-\alpha_N}}{d_L^{-\alpha_L}}}\right) \prod_{i: \mathbf{X}_i \in \Phi'_L} \left(\frac{m}{m + \frac{\varepsilon\gamma d_L'^{-\alpha_L}}{d_L^{-\alpha_L}}}\right)^m \quad (55)$$

The  $b^{\text{th}}$  moment can be given as  $M_{bL}''(d_L) = \mathbb{E}_{\Phi_b, \Phi_U}[(P'_{SL}(\gamma))^b]$ . The product is taken over the points in the PPP  $\Phi_U$ . Therefore, we first simplify the expression by taking the expectation over  $\Phi_b$  inside the product and then taking the expectation over  $\Phi_U$ . The final expression, which involves expectations over both  $\Phi_b$  and  $\Phi_U$  is given as

$$M''_{bL}(d_L) = \exp\left(\frac{-\gamma\sigma_N b}{P_u K d_L^{-\alpha_L}}\right) \mathbb{E}_{\Phi_N} \left[ \prod_{i: \mathbf{X}_i \in \Phi_N} \mathbb{E}_{\Phi_b} \left( \frac{1}{1 + \frac{\gamma d_N^{-\alpha_N}}{d_L^{-\alpha_L}}} \right)^b \right] \mathbb{E}_{\Phi_L} \left[ \prod_{i: \mathbf{X}_i \in \Phi_L} \mathbb{E}_{\Phi_b} \left( \frac{m}{m + \frac{\varepsilon\gamma d_L'^{-\alpha_L}}{d_L^{-\alpha_L}}} \right)^{mb} \right] \quad (56)$$

Taking the inner expectation wrt to  $\Phi_b$  for the NLoS case,

$$L_S(\sqrt{x^2 + t^2}, t) \left( \frac{1}{1 + \frac{\gamma(\sqrt{x^2 + t^2})^{-\alpha_L}}{z^{-\alpha_L}}} \right)^b + N_S(\sqrt{x^2 + t^2}, t) \left( \frac{1}{1 + \frac{\gamma(\sqrt{x^2 + t^2})^{-\alpha_N}}{z^{-\alpha_L}}} \right)^b \quad (57)$$

Taking the inner expectation wrt to  $\Phi_b$  for the LoS case,

$$L_S(\sqrt{x^2 + t^2}, t) \left( \frac{m}{m + \frac{\varepsilon\gamma(\sqrt{x^2 + t^2})^{-\alpha_L}}{z^{-\alpha_L}}} \right)^{mb} + N_S(\sqrt{x^2 + t^2}, t) \left( \frac{m}{m + \frac{\varepsilon\gamma(\sqrt{x^2 + t^2})^{-\alpha_N}}{z^{-\alpha_L}}} \right)^{mb}, \quad (58)$$

where  $L_S(x, y)$  is the probability that the UAV-BS at  $(x, y)$  is in LoS and  $N_S(x, y)$  is the probability that the UAV-BS at  $(x, y)$  is in NLoS. Next, we take an expectation over the height of the UAV-BSs for two cases of  $d_L$ .

Similarly, expectation over height is applied to the LoS case as well. Applying PGFL for the 2-D locations of the LoS UAV-BS and NLoS UAV-BSs of the PPP [45], the above equation can be written as (19) and (20). Taking an expectation over  $d_L$  and multiplying the probability of associating to LoS UAV-BS  $A_L$  gives the  $b^{th}$  moment of the CSP of associating to LoS UAV-BS as given in (18).

## REFERENCES

- [1] R. Arshad, L. Lampe, H. ElSawy, and M. J. Hossain, "Integrating UAVs into existing wireless networks: A stochastic geometry approach," *2018 IEEE Globecom Workshops (GC Wkshps)*, pp. 1–6, 12 2018.
- [2] Xiao, Zhenyu, and et al., "A survey on millimeter-wave beamforming enabled uav communications and networking," *IEEE Communications Surveys & Tutorials* 24.1 (2021), pp. 557–610, 11 2021.
- [3] L. Zhang, A. Celik, S. Dang, and B. Shihada, "Energy-efficient trajectory optimization for uav-assisted iot networks," *IEEE Transactions on Mobile Computing* (2021), Apr 2021.
- [4] Cai, Yuanxin, and et al., "Resource allocation and 3D trajectory design for power-efficient IRS-assisted UAV-NOMA communications," *IEEE Transactions on Wireless Communications* (2022), Jun 2022.
- [5] Gapeyenko, Margarita, and et al., "Line-of-sight probability for mmwave-based uav communications in 3d urban grid deployments," *IEEE Transactions on Wireless Communications* 20.10 (2021), Apr 2021.
- [6] Semiari, Omid, and et al., "Caching meets millimeter wave communications for enhanced mobility management in 5G networks," *IEEE Transactions on Wireless Communications* 17.2 (2017), pp. 779–93, Nov 2017.
- [7] R. Zhang, R. Lu, X. Cheng, N. Wang, and L. Yang, "A uav-enabled data dissemination protocol with proactive caching and file sharing in V2X networks," *IEEE Transactions on Communications*, pp. 3930–3942, June 2021.
- [8] Zhao, Jianwei, and et al., "Efficient deployment with geometric analysis for mmwave uav communications," *IEEE Wireless Communications Letters* 9.7, Mar 2020.
- [9] Wang, Siming, and et al., "Low-latency caching with auction game in vehicular edge computing," *2017 IEEE/CIC International Conference on Communications in China (ICCC)*, Oct 2017.
- [10] A. Fotouhi, H. Qiang, M. Ding, M. Hassan, L. G. Giordano, A. Garcia-Rodriguez, and J. Yuan, "Survey on UAV cellular communications: Practical aspects, standardization advancements, regulation, and security challenges," *IEEE Communications Surveys & Tutorials*, vol. 21.4, pp. 3417–3442, March 2019.
- [11] X. Zhang and L. Duan, "Fast deployment of uav networks for optimal wireless coverage," *IEEE Transactions on Mobile Computing* 18.3, pp. 588–601, May 2018.
- [12] Apostolidis, S. D., and et al., "Cooperative multi-uav coverage mission planning platform for remote sensing applications," *Autonomous Robots* 46.2, pp. 373–400, Feb 2022.
- [13] Hu, Wenjian, and et al., "Multi-uav coverage path planning: A distributed online cooperation method," *IEEE Transactions on Vehicular Technology* 72.9, pp. 11 727–40, Apr 2023.
- [14] RR, Neetu, and et al., "Cache enabled UAV hetnets: Access-xhaul coverage analysis and optimal resource partitioning," *IEEE Transactions on Cognitive Communications and Networking*, Oct 2023.
- [15] M. Matracia, M. A. Kishk, and M.-S. Alouini, "Uav-aided post-disaster cellular networks: A novel stochastic geometry approach," *IEEE Transactions on Vehicular Technology* 72.7, pp. 9406–18, Feb 2023.
- [16] Qin, Yujie., and et al., "Stochastic geometry-based trajectory design for multi-purpose uavs: package and data delivery," *IEEE Transactions on Vehicular Technology*, Oct 2023.
- [17] T. Bai, R. Vaze, and R. W. Heath, "Analysis of blockage effects on urban cellular networks," *IEEE Transactions on Wireless Communications*, pp. 5070–83, June 2014.
- [18] W. Tang, H. Zhang, and Y. He, "Performance analysis of power control in urban UAV networks with 3D blockage effects," *IEEE Transactions on Vehicular Technology*, vol. 71, pp. 626–638, Jan 2022.
- [19] Cunyan, Ma, and et al., "Coverage analysis of single-swarm mmwave uav networks under multiple types of blockages," *IEEE Transactions on Communications*, June 2024.
- [20] Le, Yang, and et al., "Fine-grained analysis of reconfigurable intelligent surface-assisted mmwave networks," *IEEE Transactions on Communications*, Jan 2022.
- [21] Yixiao, Gu, and et al., "The meta distribution of task offloading in stochastic mobile edge computing networks," *IEEE Transactions on Vehicular Technology*, Nov 2022.
- [22] F. Habibi, Danufane, and et al., "Analysis of the delay distribution in cellular networks by using stochastic geometry," *IEEE Open Journal of the Communications Society*, Nov 2023.
- [23] Shi, Minwei, and et al., "The meta distribution of SINR in UAV-assisted cellular networks," *IEEE Transactions on Communications*, vol. 71, no. 2, Feb 2023.
- [24] Yujie, Qin, and et al., "On the downlink sinr meta distribution of uav-assisted wireless networks," *IEEE Transactions on Communications*, Nov 2023.
- [25] Zhe, Wang, and et al., "Rate meta distribution of downlink base station cooperation for cellular-connected uav networks," *IEEE Communications Letters*, Feb 2023.
- [26] Arshad, Rabe, and et al., "Velocity-aware handover management in two-tier cellular networks," *IEEE Transactions on Wireless Communications* 16.3, 2017.
- [27] Jingwen, Bai, and et al., "Route-aware handover enhancement for drones in cellular networks," *2019 IEEE Global Communications Conference (GLOBECOM)*. IEEE, pp. 1–6, Dec 2019.
- [28] Wei, Bao, and et al., "Stochastic geometric analysis of user mobility in heterogeneous wireless networks," *IEEE Journal on Selected Areas in Communications* 33.10 (2015), pp. 2212–25, May 2015.
- [29] Ahmad, A. A., and et al., "A comprehensive survey on handover management for vehicular ad hoc network based on 5g mobile networks technology," *Transactions on Emerging Telecommunications Technologies* 30.3 (2019), 2019.
- [30] K. Tokuyama, T. Kimura, and N. Miyoshi, "Periodic handover skipping in cellular networks: Spatially stochastic modeling and analysis," *IEEE Transactions on Wireless Communications* 23.1, May 2023.
- [31] Zhou, Siyuan, and et al., "Handover and coverage analysis in 3d mobile uav cellular networks," *IEEE Internet of Things Journal* (2024), May 2024.
- [32] RR, Neetu, and et al., "Performance analysis of cache-enabled handover management for vehicular networks," *IEEE Transactions on Network Science and Engineering*, Oct 2023.
- [33] Neetu, RR, and et al., "Analysis of handover rate and coverage performance of mobile users in uav networks," *2024 IEEE 99th Vehicular Technology Conference (VTC2024-Spring)*, 2024.
- [34] M. Haenggi, "Stochastic geometry for wireless networks," Cambridge, U.K.: Cambridge Univ. Press, 2012, 2012.
- [35] Lazar, R.G., and et al., "Simulated and practical approach to assess the reliability of the 5G communications for the Uu interface," *2022 14th International Conference on Communications (COMM)*, pp. 1–6, June 2022.
- [36] A. Fouda, A. S. Ibrahim, I. Guvenc, and M. Ghosh, "UAV-based in-band integrated access and backhaul for 5G communications," *2018 IEEE 88th Vehicular Technology Conference (VTC-Fall)*, pp. 1–5, Aug 2018.
- [37] S. N. Chiu, D. Stoyan, W. S. Kendall, and J. Mecke, *Stochastic geometry and its applications*. John Wiley & Sons, 2013.
- [38] Le, N. Phuc, and et al., "Energy-harvesting aided unmanned aerial vehicles for reliable ground user localization and communications under lognormal-nakagami-m fading channels," *IEEE Transactions on Vehicular Technology* 70.2 (2021), Jan 2021.
- [39] G. Ghatak, S. S. Kalamkar, and Y. Gupta, "Radar detection in vehicular networks: Fine-grained analysis and optimal channel access," *IEEE Transactions on Vehicular Technology* 71.6 (2022), pp. 6671–81, Mar 2022.
- [40] 3GPP, "NR; user equipment (UE) radio transmission and reception; Part 2: Range 2 standalone," *3rd Generation Partnership Project (3GPP), TS 38.101-2, Version 15.9.1.*, April 2020.
- [41] Azimi-Abarghouyi, S. Mohammad, and et al., "Stochastic geometry modeling and analysis of finite millimeter wave wireless networks," *IEEE Transactions on Vehicular Technology* 68.2 (2018), Nov 2018.
- [42] M. Di Renzo and P. Guan, "Stochastic geometry modeling of coverage and rate of cellular networks using the gil-pelaez inversion theorem," *IEEE Communications Letters*, vol. 18, pp. 1575–1578, Sept 2014.
- [43] Kalamkar, S. S., and et al., "Beam management in 5G: A stochastic geometry analysis," *IEEE Transactions on Wireless Communications* 21.4 (2021), pp. 2275–2290, Sep 2021.
- [44] E. Kalantari, M. Z. Shakir, and A. Yongacoglu, *Backhaul-aware robust 3D drone placement in 5G+ wireless networks*, pp. 109–114, 05 2017.
- [45] M. Haenggi, "Stochastic geometry for wireless networks," Cambridge, U.K.: Cambridge Univ. Press, 2012, 2012.